SF2A 2014
J. Ballet, F. Bournaud, F. Martins, R. Monier and C. Reylé (eds)

TIME EVOLUTION OF A VISCOUS PROTOPLANETARY DISK WITH A FREE GEOMETRY AND REALISTIC OPACITIES.

K. Baillié[1] and S. Charnoz[1]

Abstract. Aiming to model the favorable conditions for planetary formation, we have designed a hydrodynamical numerical model for the spreading of protoplanetary disks based on a self-consistent coupling between the disk thermodynamics, photosphere geometry and dynamics (Baillié & Charnoz., 2014, ApJ 786, 35). We retrieved the recurrent observational properties of protoplanetary disks around young Classical T Tauri type stars. One of the novelty of our approach lies in the proper treatment of the disk geometry, leading to the presence of non-irradiated zones. In addition, we show the importance of the physical composition of the disk: using a full-opacity model, our disk temperature takes into account the various changes of phases experienced by the different components of our gas-dust disk. This is crucial for estimating the resonant torques that a potential planet would experience in an evolved disk: these corotation and Lindblad torques are very sensitive to the discontinuities in surface-mass density and temperature gradients. From these torques, we show that there are some preferential zones for planetary embryos to accumulate and some regions could be totally depleted in planetary cores.

Keywords: Protoplanetary disks, Planets and satellites: formation, Planet-disk interactions, Accretion disks, Planets and satellites: dynamical evolution and stability, Hydrodynamics

1 Introduction

Recent observations of young star environments were able to provide physical constraints on protoplanetary disks from different regions. For example, Isella et al. (2009) analyzed the Taurus region while Andrews et al. (2009, 2010) focused on the Orion and Ophiuchus regions. While they noticed some common characteristics in regions that are not genetically related (in particular in the asymptotic behaviours of the surface mass density or pressure scale height profiles), numerical simulations from Baillié & Charnoz (2014) were able to retrieve these properties. Their viscous spreading hydrodynamical code involves coupling the photosphere geometry, the disk thermodynamics and its dynamics. In the present work, we improve this code by considering the disk composition and its evolution with the midplane temperature. We then use the evolved disks generated by this code to build migration torque maps for a putative planetary core within the disk. These torques are composed of a Lindblad contribution and a corotation contribution. Some places in the disk midplane seem to be able to accumulate planetary embryos while some others seem to be totally depleted in planets.

2 Model

2.1 Dynamical and thermodynamical evolution

The present numerical model is based on the hydrodynamical code described in Baillié & Charnoz (2014), following the viscous evolution of a viscous α disk (Shakura & Sunyaev 1973). Most of the usual asumptions are removed: we follow the disk evolution from an already formed Minimum Mass Solar Nebula and not just its final steady state. We jointly calculate the photosphere geometry: the angle at which the photosphere sees the star is governing the amount of energy that the photosphere is receiving from the star. Therefore, the disk is not only heated by viscous heating but also by stellar irradiation. The iterative process calculating the temperature also calculates a consistent photosphere height, therefore coupling the disk geometry with the disk

[1] Laboratoire AIM, Université Paris 7 Denis Diderot, CEA, CNRS, 91191 Gif-sur-Yvette, France

Elements	Condensation/Sublimation Temperature
Water ice	160 K
Volatile Organics	275 K
Refractory Organics	425 K
Troilite (FeS)	680 K
Olivine, pyroxene ([Fe,Mg] silicates)	1500 K

Table 1. Phase changes temperatures affecting the disk gas opacity.

thermodynamics, which is also linked to the dynamical evolution through the viscosity, as detailed in Equation 2.1 (Lynden-Bell & Pringle 1974) obtained from the mass and angular momentum conservation.

$$\frac{\partial \Sigma(r,t)}{\partial t} = \frac{3}{r}\frac{\partial}{\partial r}\left(\sqrt{r}\,\frac{\partial}{\partial r}\left(\nu(r,t)\,\Sigma(r,t)\,\sqrt{r}\right)\right) \tag{2.1}$$

2.2 Opacity model

The main elements of the disk dust are listed in Table 1 with their sublimation temperatures. As the midplane temperature varies accross the protoplanetary disk, the physical phases of the various elements change as well. This affects the disk opacity which in turn affects the temperature. Therefore, we tabulate the dust opacity as a function of the temperature and we use this updated local opacity in our iterative process for the determination of the temperature and geometry. We use the tabulated values from Semenov et al. (2003) summarized in Figure 1.

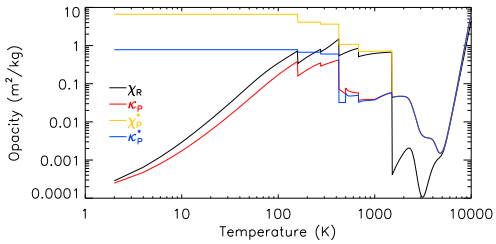

Fig. 1. Opacity variations with local temperature. Black: Rosseland mean opacity in extinction. Red: Planck mean opacity in absorption. Yellow: Planck mean opacity in extinction at stellar irradiation temperature. Blue: Planck mean opacity in absorption at stellar irradiation temperature.

The various opacities show very abrupt drops around the sulbimation temperatures of the dust elements.

3 Viscous evolution

Figure 2 shows the evolution of the surface mass density and temperature radial profiles as the disk viscously spreads. Previous conclusions form Baillié & Charnoz (2014) are retrieved: the disk reaches a steady state in a few million years, characterized by a uniform mass flux and a shallower surface mass density profile than initially. The asymptotic trends also recall the observations as we tend to $\Sigma \propto r^{-1}$.

3.1 Detailed temperature profile

The temperature remains mainly decreasing with the increasing radial distance. The disk appears to cool down as it ages. The thermal profiles reveal temperature plateaux coinciding with the sublimation temperatures reported in Table 1. The usual snow and sublimation lines are therefore enlarged and we may define a snow region in place of a snow line.

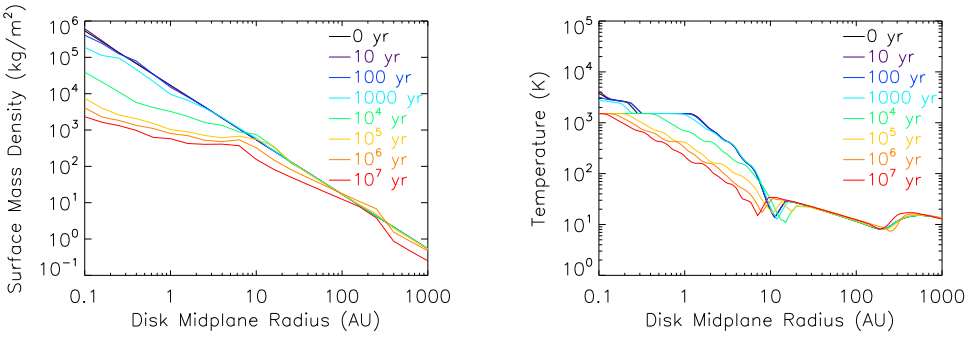

Fig. 2. Left: Surface mass density radial profile evolution for an initial minimum mass solar nebula in the case of a self-consistently calculated geometry with a full continuous model of opacities. **Right:** Corresponding mid-plane temperature radial profile evolution.

4 Migration torques

An already formed planetary embryo exchanges angular momentum with the disk (Goldreich & Tremaine 1979; Ward 1988; Artymowicz 1993; Jang-Condell & Sasselov 2005) due to the resonances excited by the planet in the disk. The planet exerts a torque on the disk and therefore the disk exerts an opposite torque on the planet. We assume that the disk structure is not modified by the presence of the planet.

4.1 Lindblad torques

We identify the Linblad resonances with a planet located at r_P by their wavenumber $m(r) = \sqrt{\frac{\kappa^2(r)}{(\Omega(r)-\Omega(r_P))^2 - \frac{c_s^2(r)}{r^2}}}$ where $c_s(r)$ is the local sound speed as defined in BC14 and $\kappa(r)$ is the epicyclic frequency. We use here the approach of Ward (1997) and Hasegawa & Pudritz (2011) who considered m as a continuous variable, function of the radius r and defined a midplane torque density exerted by the disk on the planet:

$$\frac{\mathrm{d}^2\Gamma}{\mathrm{d}z\mathrm{d}r}(r) = \epsilon\, 2\, q^2\, G\, M_* \left(\frac{r}{r_P}\right)^2 \frac{m^4}{(1+4\xi^2)} \frac{\Sigma(r)\,\psi^2}{h_{pres}(r)} \tag{4.1}$$

where $\epsilon = +1$ for $r > r_P$ and $\epsilon = -1$ for $r < r_P$, $q = \frac{M_P}{M_*}$, $\xi(r) = \frac{m(r)\, c_s(r)}{r\,\kappa(r)}$ and ψ is defined by $\psi = \left(1+\frac{r_P}{r}\right)\frac{K_1(\Lambda)}{2} + \left(\frac{\epsilon}{2m} + 2\sqrt{1+\xi^2}\right)\frac{K_0(\Lambda)}{\sqrt{r/r_P}}$, where K_i is the modified Bessel function of the second kind of order i and $\Lambda = m\frac{\left|\frac{r}{r_P}-1\right|}{\sqrt{\frac{r}{r_P}}}$. Thus, it is possible to integrate the Lindblad resonant torque density over r.

4.2 Corotation torques

Using the formulas of Paardekooper et al. (2010) and Bitsch et al. (2014), we can estimate the entropic and barotropic corotation torque contributions:

$$\Gamma_{\mathrm{hs,entro}} = -\frac{\Gamma_0(r_P)}{\gamma^2}\, 7.9 \left(-\frac{\partial \ln T}{\partial \ln r}(r_P) + (\gamma-1)\frac{\partial \ln \Sigma}{\partial \ln r}(r_P)\right) \tag{4.2}$$

$$\Gamma_{\mathrm{hs,baro}} = -\frac{\Gamma_0(r_P)}{\gamma} 1.1 \left(\frac{\partial \ln \Sigma}{\partial \ln r}(r_P) + \frac{3}{2}\right) \tag{4.3}$$

with $\gamma = 1.4$, the adiabatic index, $\Gamma_0(r_P) = \left(\frac{q}{h}\right)^2 \Sigma(r_P)\, r_P^4\, (\Omega(r_P))^2$, $h = \frac{h_{pres}(r_P)}{r_P}$, and $\Omega(r_P)$ the keplerian angular velocity at the planet position in the disk.

4.3 Planetary traps and deserts

The total torque exerted by the disk on the planet is then given by $\Gamma_{\rm tot} = \Gamma_{\rm Lindblad} + \Gamma_{\rm hs,entro} + \Gamma_{\rm hs,baro}$. This total torque strongly depends on the temperature and surface mass density gradients. A negative total torque reflects an inward planetary migration whereas a positive sign shows an outward migration. Figure 3 shows the total torque exerted by the disk on a planet located at a given radial distance r from the star after 1 million years of evolution of the protoplanetary disk. While the total torque is negative everywhere in the case of a constant opacity model, structures appear when the opacity takes into account the dust composition: 0-torque lines appear and define a diverging radius around 10 AU where the region is depleted in planets (planetary desert), and a converging radius around 16 AU where planets can accumulate (planetary trap).

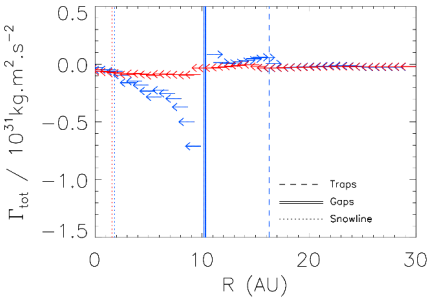

Fig. 3. Total torque exerted by the disk on a $10M_{\rm Earth}$-planet (red: constant opacity model; blue: full opacity model).

5 Conclusions and perspectives

The proper consideration of the disk composition and the physical phase of each element generates temperature irregularities (temperature plateaux, peaks and troughs) that could significantly affect the migration torques exerted by the disk on a putative planet. With these refinements, it appears possible to actually trap planets at a specific radius, or to clear a specific position of all planetesimals. After 1 Myr, we identify a planetary trap around 16 AU and a planetary desert around 10 AU. Other sources of irregularities beyond the scope of the present paper could also generate potential torque inversion and therefore planet trapping: radial variations of the viscous turbulence α, presence of deadzones, multiple-planet systems ...

This work was supported by IDEX Sorbonne Paris Cité. We acknowledge the financial support from the UnivEarthS Labex program of Sorbonne Paris Cité (ANR-10-LABX-0023 and ANR-11-IDEX-0005-02).

References

Andrews, S. M., Wilner, D. J., Hughes, A. M., Qi, C., & Dullemond, C. P. 2009, ApJ, 700, 1502
Andrews, S. M., Wilner, D. J., Hughes, A. M., Qi, C., & Dullemond, C. P. 2010, ApJ, 723, 1241
Artymowicz, P. 1993, ApJ, 419, 155
Baillié, K. & Charnoz, S. 2014, ApJ, 786, 35
Bitsch, B., Morbidelli, A., Lega, E., & Crida, A. 2014, A&A, 564, A135
Goldreich, P. & Tremaine, S. 1979, ApJ, 233, 857
Hasegawa, Y. & Pudritz, R. E. 2011, MNRAS, 417, 1236
Isella, A., Carpenter, J. M., & Sargent, A. I. 2009, ApJ, 701, 260
Jang-Condell, H. & Sasselov, D. D. 2005, ApJ, 619, 1123
Lynden-Bell, D. & Pringle, J. E. 1974, MNRAS, 168, 603
Paardekooper, S.-J., Baruteau, C., Crida, A., & Kley, W. 2010, MNRAS, 401, 1950
Semenov, D., Henning, T., Helling, C., Ilgner, M., & Sedlmayr, E. 2003, A&A, 410, 611
Shakura, N. I. & Sunyaev, R. A. 1973, A&A, 24, 337
Ward, W. R. 1988, Icarus, 73, 330
Ward, W. R. 1997, Icarus, 126, 261